THE JOURNAL OF PHYSICAL CHEMISTRY C

Article

pubs.acs.org/JPCC

Molecular Dynamics Simulation of Ice Indentation by Model Atomic Force Microscopy Tips

Julian Gelman Constantin[†]

Departamento de Física de la Materia Condensada, Centro Atómico Constituyentes, Comisión Nacional de Energía Atómica (CNEA), San Martín, B1650KNA Buenos Aires, Argentina

Instituto de Química Física de los Materiales, Medio Ambiente y Energía (INQUIMAE), Facultad de Ciencias Exactas y Naturales, Universidad de Buenos Aires, Pabellón II, Ciudad Universitaria, C1428EGA Buenos Aires, Argentina

Marcelo A. Carignano*

Qatar Environment and Energy Research Institute, Hamad Bin Khalifa University, Qatar Foundation, P.O. Box 5825, Doha, Qatar

Horacio R. Corti

Departamento de Física de la Materia Condensada, Centro Atómico Constituyentes, Comisión Nacional de Energía Atómica (CNEA), San Martín, B1650KNA Buenos Aires, Argentina

Instituto de Química Física de los Materiales, Medio Ambiente y Energía (INQUIMAE), Facultad de Ciencias Exactas y Naturales, Universidad de Buenos Aires, Pabellón II, Ciudad Universitaria, C1428EGA Buenos Aires, Argentina

Igal Szleifer

Department of Biomedical Engineering, Department of Chemistry, Chemistry of Life Processes Institute, Northwestern University, 2145 Sheridan Road, Evanston, Illinois 60208, United States

Supporting Information

ABSTRACT: We have performed extensive molecular dynamics simulations of nanoindentation of an ice slab with model atomic force microscopy (AFM) tips. We found the presence of a quasi-liquid layer between the tip and the ice for all explored indentation depths. For the smallest tip studied (R = 0.55 nm), the force versus indentation depth curves present peaks related to the melting of distinct monolayers of ice, and we were able to calculate the work (free energy) associated with it. For a larger tip (R = 1.80 nm) having a size not commensurate with the average monolayer thickness, we did not find a clear structure in force curves. This work can help guide the interpretation of experimental AFM indentation of ice and other crystalline solids. More specifically, it provides guidelines for tip sizes where layer-by-layer melting can be achieved and for the order of magnitude of forces that need to be detected.

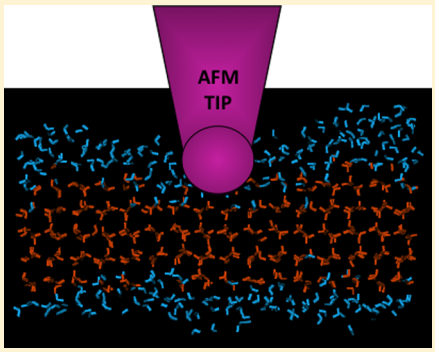

I. INTRODUCTION

Premelting at the interface with air is a feature of many crystalline solids; however, the case of ice is of paramount interest because of the environmental consequences in polar stratospheric clouds,[1] snow dynamics on the Earth's surface, oceans, and comets.[2,3] The existence of a quasi-like layer (QLL) at the ice−air interface, first proposed by Michael Faraday in 1850 to explain the regelation phenomena,[4] was confirmed through several experimental techniques,[2] including atomic force microscopy (AFM).[5−9]

AFM results yield a premelted layer much ticker than that obtained by molecular dynamics simulations[10−13] or thermodynamics models,[3] which predict a thickness of the QLL smaller than 2 nm for ice supercooling higher than 0.3 K. Because this technique involves the interaction of a nanosized tip with the disorder layer on ice, it is uncertain whether AFM measures the thickness of the QLL at the ice−air interface, the QLL between the tip and the ice, or a combination of both. It is also unknown if the tip could induce pressure melting of the ice beneath the QLL. Butt et al.[7] suggested that the AFM tip induces plastic deformation on ice after the jump-in through the QLL, while Pittenger et al.[8] proposed that at a low tip penetration speed

Received: October 19, 2015
Revised: November 5, 2015

DOI: 10.1021/acs.jpcc.5b10230
J. Phys. Chem. C XXXX, XXX, XXX−XXX

the pressure under the tip is not high enough for melting ice; however, melting could be induced by the tip−ice interactions at the interface. The resulting QLL squeezes out of the region between the tip and the ice during indentation. Li and Somorjai[14] have reviewed the QLL experimental AFM studies and concluded that the existence of a QLL between the penetrating AFM tip and the solid ice is still an open question. Thus, a careful analysis of the interaction of a nanosized model tip with the ice surface could shed some light on the perturbation of the QLL around the tip, the structure of water beneath the tip upon indentation, and the characteristics of the ice melting induced by the tip.

To the best of our knowledge, this is the first molecular dynamics simulation of ice nanoindentation. Bonner and Baratof[15] studied indentation of tiol self-assembled monolayers on gold, using a gold deformable pyramidal cluster as a model tip. They observed a jump-in due to attractive interactions, and some molecular detail of the repulsive interaction between the tip and individual tiol molecules. Buldum et al.[16] modeled a pyramidal silicon tip. The obtained force curve against a silicon substrate showed peaks that could be associated with the crystalline structure of the tip. Chandross et al.[17] performed extensive simulations with SiO_2 model tips of three different radii of curvature (3, 10, and 30 nm) and a self-assembled monolayer of alkylsilanes on silica. It allowed them to compare effective contact areas against the values predicted by simple mechanical models frequently used to analyze polymer indentation curves. They also studied the effect of velocity but concluded that simulation velocities were too high compared with experimental ones.

In this article, we present extensive atomistic molecular dynamics (MD) simulations of the ice−vapor interface in contact with two different model AFM tips at both the basal and the primary prismatic planes of ice. The aim is to gain an understanding of molecular-scale effects influencing AFM indentation on ice. We found a thin QLL in contact with the tip during indentation, which supports previous interpretation of AFM experiments.[8] The smallest simulated tip allowed us to calculate the free energy associated with a layer-by-layer local melting of ice from force versus distance curves, whereas for the larger tip, we could not attain that level of detail. Our simulation results can provide guidelines for tip sizes appropriate for achieving monolayer melting in AFM indentations, as well as the order of magnitude of forces that need to be detected in such experiments.

II. THEORETICAL METHODS

All-atom MD simulations were conducted in the *NVT* ensemble using GROMACS, version 4.5.4.[18] The integration was done using the leapfrog algorithm, with a time step of 1 fs. The temperature of the simulation boxes was kept constant with a Nosé−Hoover algorithm with a relaxation time of 0.5 ps, and the SETTLE algorithm was used to maintain the water intramolecular distances and angles. Long-range electrostatics interactions were handled with the particle mesh Ewald (PME) algorithm. Water molecules were modeled with the TIP5P/Ew model,[19] a five-point (nonpolarizable) model parametrized to be used with Ewald sums. This model was chosen following a series of studies under low-temperature conditions that proved the good performance of TIP5P/Ew in terms of thermodynamic and structural properties.[20−23] In particular, the melting point of hexagonal ice (I_h^d) for that model has been estimated to be $T_m \approx (271 \pm 3)$ K.[24,25]

Recently, several authors have performed simulations of ice crystallization with methodologies that allow the use local thermostats to control temperature gradients and take into account the latent heat involved during the phase transformations.[26,27] Nevertheless (see below), experimental AFM curves are obtained at very slow speeds, allowing for full dissipation of the latent heat (or heat from the tip).[28] Namely, the experimental AFM curves are obtained under quasi-static conditions, and therefore, the use of a single thermostat to equilibrate the system is not only justified but also a convenient way to reach proper equilibrium in shorter simulation times.

A. Ice. The initial coordinates of the ice block (768 molecules) were taken from ref 29, corresponding to proton disordered phase I_h^d. The ice block was replicated and translated to create boxes large enough for the simulations. Coordinates were rotated such that the exposed face (basal or primary prismatic plane) was perpendicular to the z axes.

We simulated force curves for different solid and liquid systems, at 270 K ($T_m - T \approx 1$ K). The prefix of the names of ice systems (*Basal-3072*, *Basal-6912*, and *Prismatic-6144*) specifies the crystal face exposed to vacuum and to the tip (basal or primary prismatic), whereas the suffix is the number of water molecules in the ice simulation. Similarly, *Liquid-3512* and *Liquid-7902* are liquid water slabs of 3512 and 7902 molecules, respectively.

B. Model AFM Tips. Most common AFM tips have a truncated pyramidal shape, with a very small radius of curvature at the apex (1 nm $\lesssim R \lesssim$ 100 nm). We have modeled the tip as a sphere of radius R; therefore, for indentation depths $\zeta < R$, the results should represent approximately that of a truncated pyramidal tip. At indentation depths $\zeta > 2R$, there could be a larger difference between our results and the expected force acting on a truncated pyramidal tip. The interaction of the tip with water molecules was represented by a repulsive-only potential for tip 1:

$$V = 4\varepsilon\left(\frac{\sigma}{r - r_0}\right)^{12} \tag{1}$$

where ε and σ are the Lennard-Jones parameters and r_0 allows the radius of the sphere to shift. For tip 1, an r_0 of 0.36 nm resulted in an R of 0.55 nm (see the Supporting Information). For tip 2, we used a truncated and shifted Lennard-Jones potential:

$$V = 4\varepsilon\left[\left(\frac{\sigma}{r - r_0}\right)^{12} - \left(\frac{\sigma}{r - r_0}\right)^{6}\right] + \varepsilon \tag{2}$$

This potential is truncated at $r = r_0 + 2^{1/6}\sigma$. For tip 2, an r_0 of 1.595 nm resulted in an R of 1.80 nm. For both of the tips, we arbitrarily set ε equal to 0.7448 kJ mol^{-1} and σ equal to 0.3097 nm, same as the Lennard-Jones potential centered on the oxygen of the TIP5P/Ew model. Hence, the hardness of the potential is the same as that of TIP5P/Ew water. These Lennard-Jones parameters are very similar to those in the OPLS force field for nitrogen, a major component of some AFM tips, usually made of Si_3N_4 or Si.

This simple model allows us to capture some fundamental aspects of the interaction of a semispherical tip of a simple noncharged material and the ice−QLL system. In the future, we will increase the complexity of the model by including molecular detail, like charged hydroxyl groups that are present

DOI: 10.1021/acs.jpcc.5b10230
J. Phys. Chem. C XXXX, XXX, XXX−XXX

in most Si and Si_3N_4 surfaces, and a more complex geometry to gain further insights.

C. Force versus Distance Curves. Experimental AFM force curves are performed at speeds of ~10 μm s^{-1} corresponding to 0.001 nm every 100 ns. These speeds are prohibitively slow for computer simulations.[17,30] However, because of the short relaxation time of supercooled water at this temperature, and the slow motion of the tip, the interaction of the system and the tip can be studied quasi-statically. Therefore, all force curves presented here for both ice−QLL slabs and liquid water slabs were prepared setting up multiple (independent) simulation boxes with different tip-to-sample distances and running umbrella sampling MD simulations for each case. See the Supporting Information for additional details.

To determine the appropriate size of the ice or liquid slab for the simulations, we studied the force curves for tip 1 (R = 0.55 nm) and different liquid slabs: *Liquid-878* (with a surface area of ~3 nm × ~3 nm), *Liquid-3512* (~6 nm × ~6 nm), and *Liquid-7902* (~9 nm × ~9 nm). Results in Figure 1 showed

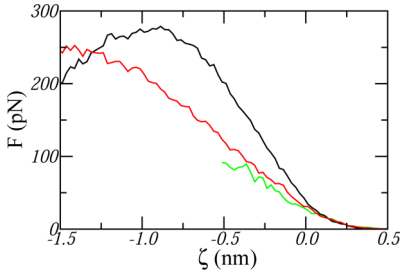

Figure 1. Average force on the AFM tip in the z direction, as a function of the distance from the tip (for tip 1, R = 0.55 nm) to the surface of the sample (liquid water slabs in all cases). ζ = 0 was arbitrarily set as described in the text: black, system *Liquid-878*; red, system *Liquid-3512*; green, system *Liquid-7902*.

that forces induced by the tip present correlations larger than the size of the box for *Liquid-878*, because increasing the section area (*Liquid-3512*) leads to a decrease in calculated forces. A further increase in system size (*Liquid-7902*) resulted in a minor decrease in forces at the expenses of a large increase in computational effort. Hence, we choose a section area of 6 nm × 6 nm for tip 1. Similarly, we simulated systems with a section of 9 nm × 9 nm for tip 2. For the primary prismatic plane, we had to increase the thickness of the ice system from *Prismatic-3072* to *Prismatic-6144*, because the thicker QLL led to complete melting of *Prismatic-3072*.

D. Order Parameters. To quantify the number of molecules in the solid and liquid phases, we used an operational hydrogen bond definition following the method of Carignano et al.[11] First, we set an oxygen−oxygen distance cutoff (r_{HB} < 0.35 nm). Second, we choose an angular cutoff for the angle among the hydrogen, the donor oxygen, and the acceptor oxygen (θ_{HB} < 15° in our case). As previously shown,[11] averaging over 20 ps the number of hydrogen bonds defined this way allows easy discrimination between the solid and liquid phases. Figure 2 shows that, for our simulations, an $\langle N_{HB}\rangle$ cutoff value of 2.9 is appropriate for discriminating between the two phases.

Additionally, we use the orientational order parameter q,[31,32] but considering only the closest three neighbors (at a distance r < 0.35 nm); hence, we renamed it q_3:

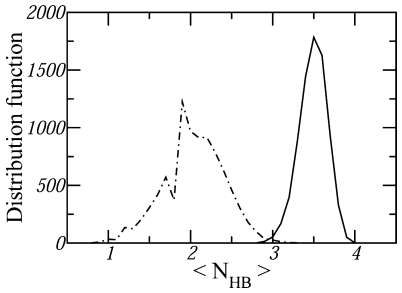

Figure 2. Time average (over 20 ps) of the number of hydrogen bonds, as defined in the text. The solid line is for bulk ice, and the dashed−dotted line is for bulk water.

$$q_3 = 1 - \frac{3}{8}\sum_{j=1}^{2}\sum_{k=j+1}^{3}\left(\cos\phi_{jk} + \frac{1}{3}\right)^2 \quad (3)$$

where ϕ_{jk} for molecule i is the angle spanned by the distance vectors r_{ij} and r_{ik} connecting the oxygen of molecule i and those of closest neighbor oxygens j and k. This parameter is unity for a perfect tetrahedral arrangement and takes lower values for other arrangements, reaching zero average for random orientations. The q_3 order parameter has the advantage over the number of hydrogen bonds, for analyzing interfaces, that it requires that the molecule have only three close neighbors. Figure 3 shows that the q_3 distribution for the inner layers of an

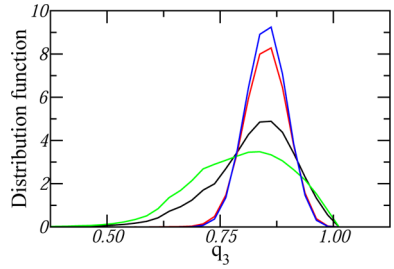

Figure 3. Results for the q_3 distribution for different systems: blue, bulk ice; green, bulk liquid water; red, inner layers of an ice−QLL slab; black, outer layers of an ice−QLL slab.

ice−QLL slab is very similar to that of bulk ice. The corresponding distribution for the outer layer shows an intermediate behavior between those of bulk ice and bulk liquid water, as it contains the mobile and frozen molecules that characterize the QLL.

III. RESULTS AND DISCUSSION

All ice slabs exposed to vacuum presented a QLL, the thickness of which depended on the exposed face of the crystal. It is convenient to refer to the thickness of the QLL in units of monolayers, which is defined as the QLL involving a number of molecules corresponding to a monolayer of ice and resulting in approximately 0.4 nm of a quasi-liquid state. For the basal plane of the crystal, the thickness of the QLL oscillated between one and two monolayers at 270 K (average of 1.5 monolayers). For the primary prismatic plane, the thickness of the QLL varied between one and three monolayers (average of 2.3 monolayers). This anisotropy has been previously observed experimentally.[33,34] Limmer and Chandler[13] have suggested that longer simulation times are necessary to equilibrate the QLL. Their results could imply that the absolute values of QLL

DOI: 10.1021/acs.jpcc.5b10230
J. Phys. Chem. C XXXX, XXX, XXX−XXX

thicknesses we report are not correct. The absolute values could also be affected by the finite thickness of the ice slab.[35] However, because the focus of this work is to analyze changes in the ice−QLL slab due to interaction with model tips, it is sufficient to attain QLL thicknesses that do not change significantly over our simulation time spans. Indeed, we found that the measured average thicknesses were stable during tens of nanoseconds once equilibration had been reached after the first two or three nanoseconds of simulation.

Figure 4 presents force versus distance curves for different systems. The blue lines represent the indentation curves of an ice−QLL slab of 3072 molecules exposing the basal plane (*Basal-3072*) to tip 1 (R = 0.55 nm). The red line is the force profile for a slab of liquid water of similar size (*Liquid-3512*). The coordinate ζ was arbitrarily set in such a way that positive values represent the distance from the ice−QLL surface to the surface of the tip, and negative values represent the approximate indentation depth. See the snapshots in the left panel of Figure 5 for a visual image of different indentation depths ζ.

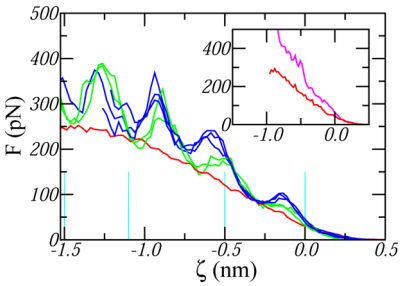

Figure 4. Average force on the AFM tip in the z direction, as a function of the tip−surface distance ζ, at 270 K: blue, ice−QLL (*Basal-3072*), tip 1, three independent simulations; green, ice−QLL (*Prismatic-6144*), tip 1, two independent simulations; red, water slab (*Liquid-3512*), tip 1. Cyan vertical lines indicate indentation depths of the representative snapshots in Figure 5. Inset: magenta line, ice−QLL (*Basal-6912*), tip 2; red line, water slab (*Liquid-7902*, tip 2).

The indentation curves for the *Basal-3072* ice slab show a clear peaked structure. It is interesting that between peaks the ice curve overlaps with that of the pure liquid water, suggesting that the peaks are related to layer-by-layer melting. Namely, on the overlapping region of the curves, the tip feels liquid water in both cases. The separation between peaks is approximately 0.44, 0.34, and 0.39 nm and is comparable to the thickness of each monolayer of ice, 0.37 nm. The three blue curves are independent simulations that show effectively identical results. The local layer-by-layer melting can be seen in the snapshots presented in the left panel of Figure 5 for different indentation positions. The green curves in Figure 4 show the indentation curves when the primary prismatic plane (*Prismatic-6144*) is exposed. The force−distance curves show the presence of peaks that are different from the ones predicted for the basal plane. The peaks for the prismatic plane show a lower amplitude as well as a slightly smaller width. However, in both cases, the indentation curves overlap with that of the liquid water between peaks. This suggests that the work of melting an ice layer locally around the tip is lower for the prismatic plane than for the basal plane. A quantitative treatment is shown below.

Next we show the effect of the tip size as obtained by simulating the indentation with tip 2 (R = 1.80 nm) and the ice−QLL system *Basal-6912*. The results are displayed in the inset of Figure 4. The clear layer-by-layer structure predicted with the smaller tip is not observed in this case. This can be rationalized in terms of the commensurability between the tip size and the thickness of the ice layer. The tip 1 radius (R = 0.55 nm) is commensurate with the ice monolayer average thickness ($d \approx 0.37$ nm), whereas for tip 2, this is no longer true. This result suggests that to observe experimentally layer-by-layer melting, the size of the AFM tip needs to be commensurate with the ice layer thickness. This is probably true for other solids, as well, and thus, it provides guidelines that will help experimentalists to select tip sizes appropriate for probing the structure of a crystalline solid.

Visualization of all the simulation trajectories (both crystal faces and both tip sizes) shows that the ice melted locally (around the tip) with an increasing indentation depth. To quantify this observation, we calculated the spatial distribution of the average number of hydrogen bonds of water molecules, $\langle N_{HB} \rangle$, for different indentation depths (right panel of Figure 5). We use the criteria that molecules with $\langle N_{HB} \rangle$ values higher than 2.9 correspond to ice and those lower values correspond to liquid water. The spatial distribution of the average number of hydrogen bonds displayed in Figure 5 shows that a liquid layer is always in contact with the tip.

To further confirm the local melting around the tip shown in Figure 5, we studied the values of the order parameter q_3 for the molecules in contact with the tip. The corresponding distribution functions are displayed in Figure 6. All the distributions are very similar to that of liquid water, which suggests that molecules in contact with the tip are in a liquidlike state. This result supports the hypothesis of Pittenger et al.[8] of the existence of a thin QLL between the tip and the ice sample at $T > 263$ K. Butt et al.[7] discarded the existence of this QLL between the tip and ice due to the necessity of assuming an "unreasonably high" viscosity for such a layer. However, there is experimental evidence that indicates that confinement can produce a significant enhancement in viscosity in some aqueous systems,[36] so in that case, our results are not in contradiction with the findings of Butt et al.

Potentials of mean force (PMF) obtained from integration of the force curves [$\mathrm{PMF}(\zeta) = -\int_{+\infty}^{\zeta} F_{\zeta'}\, d\zeta'$] show clear steps for tip 1 that correspond to the distinct peaks in Figure 4 (results shown in the Supporting Information). PMF represents the work necessary to push the AFM tip up to a certain indentation depth. The difference between the PMF of an ice−QLL system and that of a liquid system of similar size accounts for the free energy of melting (induced by the tip). Results are summarized in Table I. The column labeled as N corresponds to the difference between the number of liquidlike molecules in the crystal face in contact with the tip before and after that peak, that is, the number of molecules that melted. The other columns, W/N and W/A (where A is the measured contact area), are different attempts to normalize the work of each peak. The quotient W/N corresponds to the molar free energy of melting for the simulated ice indentation. For all peaks and for both crystal faces, W/N values are relatively small, consistent with a process close to equilibrium. The magnitude of the errors (mainly due to the uncertainty in N) is rather large and prevents a fine quantitative analysis of these values. In fact, we implemented the blocking algorithm[37] to estimate the uncertainties from the individual simulated trajectories on the magnitudes studied in this work. However, we found that that procedure seriously underestimated them. Hence, we report the

DOI: 10.1021/acs.jpcc.5b10230
J. Phys. Chem. C XXXX, XXX, XXX−XXX

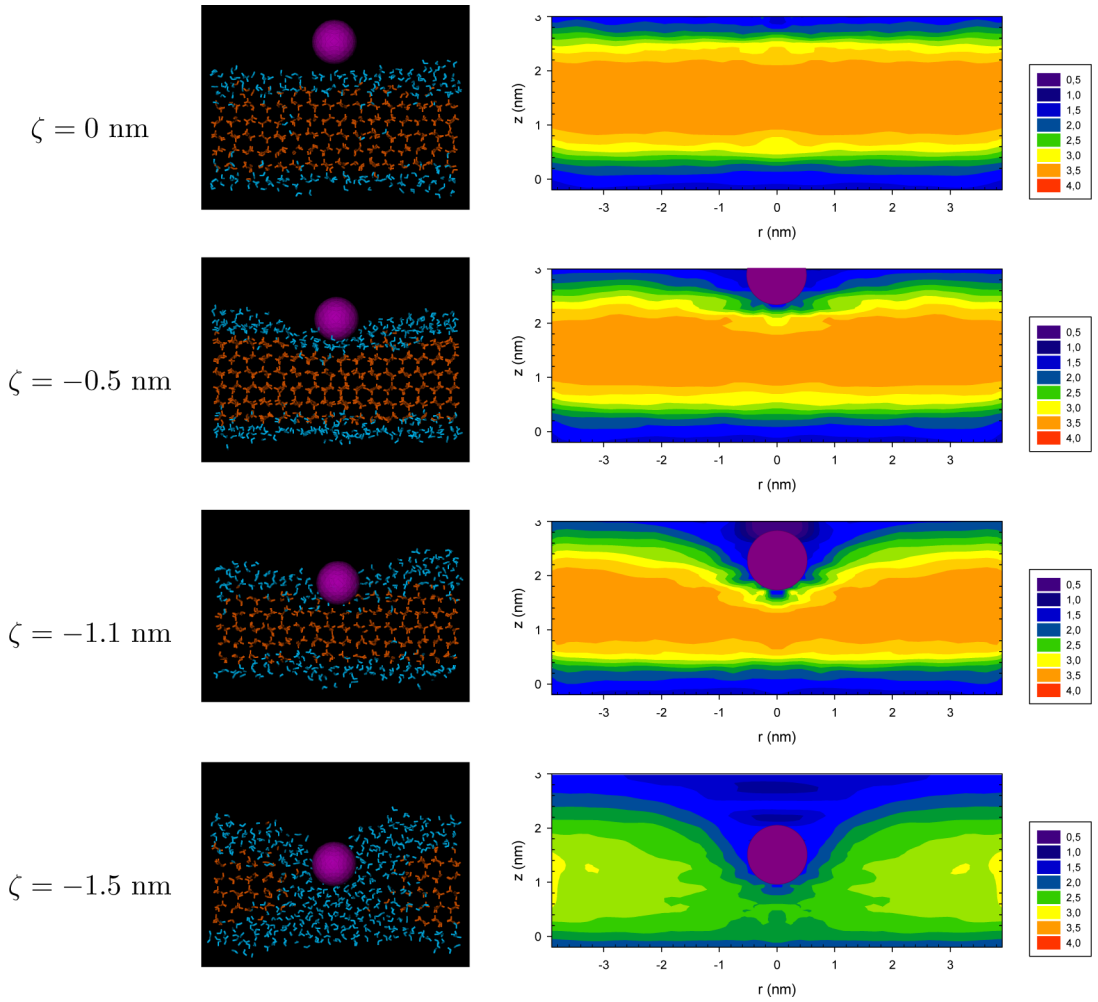

Figure 5. Left panels show representative snapshots of ice−QLL system *Basal-3072* and tip 1 (R = 0.55 nm), at 270 K, for different indentation depths. Blue-colored water molecules correspond to $\langle N_{HB} \rangle$ < 2.9. Right panels show the spatial distribution of the average number of hydrogen bonds ($\langle N_{HB} \rangle$; see the color scale at the right) of water molecules as a function of indentation depth, for the same system.

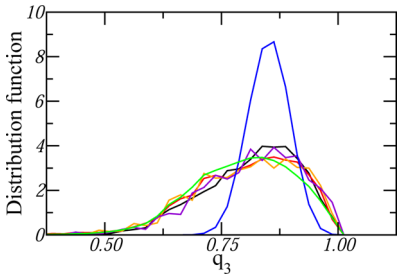

Figure 6. Results for the q_3 order parameter distribution for different systems at 270 K: blue, bulk ice; green, bulk liquid water. All other curves correspond to the molecules in contact with the tip (tip 1) for different indentation depths (between −0.8 and 0 nm), for system *Basal-3072*.

maximal difference between the averages obtained from independent simulations, as an estimate of the uncertainties.

We have performed a simple macroscopic thermodynamic calculation considering the process of pressurizing ice up to the melting equilibrium pressure (132 bar for 1 K of supercooling) and then taking the liquid to the final (upper or lower) pressure (see the Supporting Information). Results have the same order of magnitude than our PMF results: 26−35 J mol^{-1} for the first peak and 130−270 J mol^{-1} for the second peak. Even though experiments with different tip geometries and functionalization of their surfaces may shed light on additional effects, the agreement between the thermodynamic argument and the simulations suggests that pressure melting may be the dominant mechanism that induces the QLL between the tip and the solid ice during indentation.

The simulations show that the work (or free energy difference) for each melting peak is higher for the basal plane than for the primary prismatic plane. This observation is consistent with experimental evidence[33,34,38] and simple calculations[33,39] that suggest that the surface free energy of the primary prismatic plane is higher than that of the basal plane. These differences in surface free energy are also consistent with the different ice growth mechanisms for basal and primary prismatic planes.[11]

IV. CONCLUSIONS

In summary, we have performed for the first time extensive MD simulations of ice−QLL nanoindentation with two model AFM tips of two different curvature radii. Unlike most simulations of AFM indentation, we used a quasi-static approach, given the fact that experimental AFM experiments have time scales too slow to make a real-time simulation feasible. We found that indentation induces local melting of the ice near the tip. We

DOI: 10.1021/acs.jpcc.5b10230
J. Phys. Chem. C XXXX, XXX, XXX−XXX

Table I. Summary of Work (or free energy differences) for Systems *Basal-3072* and *Prismatic-6144*, Tip 1, at 270 K

	peak	W ($\times 10^{-24}$ J)	N (no. of molecules)	W/N (J mol^{-1})	W/A (kJ mol^{-1} nm^{-2})
basal	first	7.3 ± 1.6	(61−91)	(51−68)	(3.9−5.8)
	second	21.8 ± 1.6	(27−83)	(150−520)	(6.0−6.8)
	third	21.8 ± 2.3	(38−140)	(100−310)	(4.3−5.3)
prismatic	first	3.5 ± 0.9	(0−40)	(0−66)	(1.7−3.6)
	second	10.7 ± 1.4	(61−104)	(54−118)	(3.3−4.8)
	third	15.8 ± 3.1	(0−65)	(0−174)	(2.8−4.9)
	fourth	28.6 ± 3.7	(38−84)	(177−507)	(4.1−5.9)

used different order parameters to confirm the presence of a QLL between the tip and the ice sample for all explored indentation depths, endorsing the analysis by Pittenger et al.[8] of experimental AFM force curves. We found that for a small tip (R = 0.55 nm), force curves present peaks, associated with the local melting of ice around the tip. We determined the associated total work (free energy) of melting through the calculation of the PMF. For a larger tip (R = 1.80 nm), the size is no longer commensurate with the average monolayer thickness and we do not find a clear structure in force curves or PMF results. Our results provide guidelines for choosing tip sizes appropriate to achieve monolayer melting in indentation experiments of solid layers, and the order of magnitude of forces that need to be distinguished from the noise. Our simulations provide molecular-level insight for resolving the controversy about the interpretation of experimental AFM curves.[5,6,8] Further simulations with modified tips with different geometries and chemical detail will give an estimation of the magnitude of different forces involved in experiments (capillary forces, melting, etc.), which will help in the selection of the correct model to get quantitative results from experiments.

■ ASSOCIATED CONTENT

Supporting Information

The Supporting Information is available free of charge on the ACS Publications website at DOI: 10.1021/acs.jpcc.5b10230.

Additional data (PDF)

■ AUTHOR INFORMATION

Corresponding Author

*E-mail: mcarignano@qf.org.qa.

Present Address

†J.G.C.: Grupo de Química Atmosférica, Centro Atómico Constituyentes, Comisión Nacional de Energía Atómica (CNEA), San Martín, B1650KNA Buenos Aires, Argentina.

Notes

The authors declare no competing financial interest.

■ ACKNOWLEDGMENTS

H.R.C. is member of Consejo Nacional de Investigaciones Científicas y Técnicas (CONICET). J.G.C. is thankful for a fellowship from CONICET and a Fulbright/Bunge & Born grant. I.S. acknowledges financial support from National Science Foundation Grant CBET-1403058.

■ REFERENCES

(1) Molina, M. J.; Zhang, R.; Wooldridge, P. J.; McMahon, J. R.; Kim, J. E.; Chang, H. Y.; Beyer, K. D. Physical chemistry of the H_2SO_4/HNO_3/H_2O system: Implications for polar stratospheric clouds. *Science* **1993**, *261*, 1418−1416.

(2) Bartels-Rausch, T.; Jacobi, H.-W.; Kahan, T. F.; Thomas, J. L.; Thomson, E. S.; Abbatt, J. P. D.; Ammann, M.; Blackford, J. R.; Bluhm, H.; Boxe, C.; et al. A review of air/ice chemical and physical interactions (AICI): liquids, quasi-liquids, and solids in snow. *Atmos. Chem. Phys.* **2014**, *14*, 1587−1633.

(3) Dash, J. G.; Rempel, A. W.; Wettlaufer, J. S. The physics of premelted ice and its geophysical consequences. *Rev. Mod. Phys.* **2006**, *78*, 695−741.

(4) Faraday, M., XXIV. On regelation, and on the conservation of force. *Philos. Mag. Series 4* **1859**, *17*, 162−169.

(5) Petrenko, V. F. Study of the Surface of Ice, Ice/Solid and Ice/Liquid Interfaces with Scanning Force Microscopy. *J. Phys. Chem. B* **1997**, *101*, 6276−6281.

(6) Döppenschmidt, A.; Butt, H.-J. Measuring the Thickness of the Liquid-like Layer on Ice Surfaces with Atomic Force Microscopy. *Langmuir* **2000**, *16*, 6709−6714.

(7) Butt, H.-J.; Döppenschmidt, A.; Hüttl, G.; Müller, E.; Vinogradova, O. I. Analysis of plastic deformation in atomic force microscopy: Application to ice. *J. Chem. Phys.* **2000**, *113*, 1194−1203.

(8) Pittenger, B.; Fain, S. C.; Cochran, M. J.; Donev, J. M. K.; Robertson, B. E.; Szuchmacher, A.; Overney, R. M. Premelting at ice-solid interfaces studied via velocity-dependent indentation with force microscope tips. *Phys. Rev. B: Condens. Matter Mater. Phys.* **2001**, *63*, 134102.

(9) Goertz, M.; Zhu, X.-Y.; Houston, J. Exploring the liquid-like layer on the ice surface. *Langmuir* **2009**, *25*, 6905−6908.

(10) Ikeda-Fukazawa, T.; Kawamura, K. Molecular-dynamics studies of surface of ice Ih. *J. Chem. Phys.* **2004**, *120*, 1395−1401.

(11) Carignano, M.; Shepson, P.; Szleifer, L. Molecular dynamics simulations of ice growth from supercooled water. *Mol. Phys.* **2005**, *103*, 2957−2967.

(12) Conde, M. M.; Vega, C.; Patrykiejew, A. The thickness of a liquid layer on the free surface of ice as obtained from computer simulation. *J. Chem. Phys.* **2008**, *129*, 014702.

(13) Limmer, D.; Chandler, D. Premelting, fluctuations and coarse-graining of water-ice interfaces. *J. Chem. Phys.* **2014**, *141*, 18C505.

(14) Li, Y.; Somorjai, G. A. Surface Premelting of Ice. *J. Phys. Chem. C* **2007**, *111*, 9631−9637.

(15) Bonner, T.; Baratoff, A. Molecular dynamics study of scanning force microscopy on self-assembled monolayers. *Surf. Sci.* **1997**, *377−379*, 1082−1086.

(16) Buldum, A.; Ciraci, S.; Fong, C. Y.; Nelson, J. S. Interpretation of long-range interatomic force. *Phys. Rev. B: Condens. Matter Mater. Phys.* **1999**, *59*, 5120−5125.

(17) Chandross, M.; Lorenz, C. D.; Stevens, M. J.; Grest, G. S. Simulations of Nanotribology with Realistic Probe Tip Models. *Langmuir* **2008**, *24*, 1240−1246.

(18) Hess, B.; Kutzner, C.; van der Spoel, D.; Lindahl, E. GROMACS 4: Algorithms for Highly Efficient, Load-Balanced, and Scalable Molecular Simulation. *J. Chem. Theory Comput.* **2008**, *4*, 435−447.

(19) Rick, S. W. A reoptimization of the five-site water potential (TIP5P) for use with Ewald sums. *J. Chem. Phys.* **2004**, *120*, 6085−6093.

(20) Pereyra, R. G.; Szleifer, I.; Carignano, M. A. Temperature dependence of ice critical nucleus size. *J. Chem. Phys.* **2011**, *135*, 034508.

DOI: 10.1021/acs.jpcc.5b10230
J. Phys. Chem. C XXXX, XXX, XXX−XXX

(21) Pereyra, R. G.; Bermúdez di Lorenzo, A. J.; Malaspina, D. C.; Carignano, M. A. On the relation between hydrogen bonds, tetrahedral order and molecular mobility in model water. *Chem. Phys. Lett.* **2012**, *538*, 35−38.
(22) Picasso, G. C.; Malaspina, D. C.; Carignano, M. A.; Szleifer, I. Cooperative dynamic and diffusion behavior above and below the dynamical crossover of supercooled water. *J. Chem. Phys.* **2013**, *139*, 044509.
(23) Malaspina, D. C.; di Lorenzo, A. J. B.; Pereyra, R. G.; Szleifer, I.; Carignano, M. A. The water supercooled regime as described by four common water models. *J. Chem. Phys.* **2013**, *139*, 024506.
(24) Garcia Fernandez, R.; Abascal, J. L. F.; Vega, C. The melting point of ice I_h for common water models calculated from direct coexistence of the solid-liquid interface. *J. Chem. Phys.* **2006**, *124*, 144506.
(25) Vega, C.; Abascal, J. L. F. Relation between the melting temperature and the temperature of maximum density for the most common models of water. *J. Chem. Phys.* **2005**, *123*, 144504.
(26) Razul, M. S. G.; Kusalik, P. G. Crystal growth investigations ofice/water interfaces from molecular dynamics simulations: Profile functions andaverage properties. *J. Chem. Phys.* **2011**, *134*, 014710.
(27) English, N. J. Massively parallel molecular-dynamics simulation of ice crystallisation and melting: The roles of system size, ensemble, and electrostatics. *J. Chem. Phys.* **2014**, *141*, 234501.
(28) Bluhm, H.; Inoue, T.; Salmeron, M. Friction of ice measured usinglateral force microscopy. *Phys. Rev. B: Condens. Matter Mater. Phys.* **2000**, *61*, 7760−7765.
(29) Hayward, J. A.; Reimers, J. R. Unit cells for the simulation of hexagonal ice. *J. Chem. Phys.* **1997**, *106*, 1518−1529.
(30) Szlufarska, I.; Chandross, M.; Carpick, R. W. Recent advances in single-asperity nanotribology. *J. Phys. D: Appl. Phys.* **2008**, *41*, 123001.
(31) Chau, P.-L.; Hardwick, A. J. A new order parameter for tetrahedral configurations. *Mol. Phys.* **1998**, *93*, 511−518.
(32) Errington, J. R.; Debenedetti, P. G. Relationship between structural order and the anomalies of liquid water. *Nature* **2001**, *409*, 318−321.
(33) Beaglehole, D.; Nason, D. Transition layer on the surface on ice. *Surf. Sci.* **1980**, *96*, 357−363.
(34) Furukawa, Y.; Yamamoto, M.; Kuroda, T. Ellipsometric study of the transition layer on the surface of an ice crystal. *J. Cryst. Growth* **1987**, *82*, 665−677.
(35) Bluhm, H.; Salmeron, M. Growth of nanometer thin ice films from water vapor studied using scanning polarization force microscopy. *J. Chem. Phys.* **1999**, *111*, 6947.
(36) Dhinojwala, A.; Granick, S. Relaxation Time of Confined Aqueous Films under Shear. *J. Am. Chem. Soc.* **1997**, *119*, 241−242.
(37) Flyvbjerg, H.; Petersen, H. G. Error estimates on averages of correlated data. *J. Chem. Phys.* **1989**, *91*, 461.
(38) Ketcham, W. M.; Hobbs, P. V. An experimental determination of the surface energies of ice. *Philos. Mag.* **1969**, *19*, 1161−1173.
(39) Lied, A.; Dosch, H.; Bilgram, J. H. Surface melting of ice I_h single crystals revealed by glancing angle X-ray scattering. *Phys. Rev. Lett.* **1994**, *72*, 3554−3557.

DOI: 10.1021/acs.jpcc.5b10230
J. Phys. Chem. C XXXX, XXX, XXX−XXX